A generalized Navier boundary condition for modeling contact lines using second-order conservative phase-field methods

By R. Brown, S. Mirjalili, M. Khanwale, B. Ganapathysubramanian† AND A. Mani

1. Motivation and objectives

A contact line is formed when an interface between two phases intersects a solid wall. Flows with contact lines are found in various applications, such as printing, microfluidics and flow in porous media, to name a few (Sui *et al.* 2014). A significant amount of work, spanning theory, experiment and simulation, has been done over the past several decades on this subject, and it continues to be an active research area. In particular, the proper method to simulate contact lines using computational fluid dynamics has not yet been fully resolved, though significant developments have been achieved in recent years (Sui *et al.* 2014; Snoeijer & Andreotti 2013; Mohammad Karim 2022).

This report focuses on the simulation of contact lines using the phase-field (diffuse-interface) method, which is a particular framework for modeling multiphase flows. Phase-field models involve a smooth diffused representation of the interface with an order parameter ϕ, which can be computationally resolved. The central idea is that in the asymptotic limit of the interfacial thickness of the diffuse interface going to zero, one recovers the sharp interface behavior. The sharp interface limit is reached for an interface thickness parameter that can be resolved by a mesh and leads to a smooth Eulerian description of the two-phase mixture. Despite the computationally thickened interface, phase-field models can produce physically accurate results at the sharp-interface limit(Jacqmin 1999; Mirjalili *et al.* 2017, 2019; Magaletti *et al.* 2013; Khanwale *et al.* 2020).

A popular phase-field model is the fourth-order Cahn-Hilliard equation coupled with the Navier-Stokes equations (CH-NS) (Jacqmin 1999; Abels *et al.* 2012; Khanwale *et al.* 2020). This model has been successfully used to model contact lines. After discovering that slip near moving contact lines is governed by the Generalized Navier Boundary Condition (GNBC), Qian *et al.* (2003) formulated the CH-NS model with the GNBC and found good agreement between results from the continuum CH-NS simulations and results from molecular dynamics simulations. The GNBC is a slip boundary condition in which slip is proportional to shear stress and an uncompensated Young's stress due to deviation of the contact angle from its equilibrium value (Qian *et al.* 2003). This CH-NS model with the GNBC has been further developed to accurately and efficiently model contact lines over complex geometries (Shahmardi *et al.* 2021). More recently, Yue & Feng (2011) showed that moving contact lines can be accurately simulated even with the no-slip boundary condition for mixture velocity; contact line motion occurs via the right-hand-side (RHS) flux in the Cahn-Hilliard equation. Owing to its greater popularity, much work has been done on the CH-NS model in the context of moving contact lines compared to other phase-field models. One distinguishing feature of the CH-NS model

† Department of Mechanical Engineering, Iowa State University

for modeling contact lines is that it allows for direct enforcement of the contact angle in addition to the no-flux condition because the Cahn-Hilliard equation is fourth-order in space (Jacqmin 1999; Shahmardi *et al.* 2021). In contrast, in this brief, we consider a second-order phase-field model, meaning that direct enforcement of the contact angle in the phase-field equation is not possible if the no-flux condition is also required.

The second-order model studied in this report is a conservative phase-field model, denoted as the conservative diffuse interface, or CDI (Chiu & Lin 2011; Mirjalili & Mani 2021), for which we formulate a variation of the GNBC to model contact lines. CDI offers several advantages compared to models based on the Cahn-Hilliard equation and is of significant interest in the context of incompressible and compressible multiphase flows (Mirjalili & Mani 2021; Jain *et al.* 2020; Chiu & Lin 2011). To broaden its application, its important to develop treatments that allow it to model flows with contact lines.

CDI provides a second-order governing PDE for ϕ as

$$\frac{\partial \phi}{\partial t} + \nabla \cdot (\vec{u}\phi) = \Gamma \nabla \cdot \left[\epsilon \nabla \phi - \phi(1-\phi)\hat{n}_\phi\right], \tag{1.1}$$

where Γ is a mobility parameter, ϵ is a parameter related to the interface thickness, and $\hat{n}_\phi = \frac{\nabla \phi}{|\nabla \phi|}$. The first term within the parentheses on the RHS is a diffusive flux, and the second is a sharpening flux. Note that pure phase 1 exists where $\phi = 1$ and pure phase 2 exists where $\phi = 0$. The phase-field equation is coupled with the continuity equation and the incompressible Navier-Stokes equation,

$$\nabla \cdot \vec{u} = 0, \tag{1.2}$$

$$\frac{\partial (\rho \vec{u})}{\partial t} + \nabla \cdot \left[(\rho \vec{u} - \vec{S}) \otimes \vec{u}\right] = -\nabla P + \nabla \cdot \left[\mu(\nabla \vec{u} + \nabla^T \vec{u})\right] + \vec{F}^{ST}, \tag{1.3}$$

where $\vec{S} = \Gamma(\rho_1 - \rho_2)[\epsilon \nabla \phi - \phi(1-\phi)\vec{n}_\phi]$ with ρ_1 and ρ_2 being the densities of the two phases and $\vec{F}^{ST}$ is the surface tension force, modeled using the continuum surface force (CSF) formulation: $\vec{F}^{ST} = \gamma \kappa \nabla \phi$, where the curvature is $\kappa = \nabla \cdot \hat{n}_\phi$ and γ is the surface tension coefficient between the two phases. Both the density, ρ, and viscosity, μ, are typically linear functions of ϕ [see Mirjalili *et al.* (2019); Mirjalili & Mani (2021)]. To focus on the contact line dynamics, in this work, we choose the same values for the density and viscosity of the two phases, and as a result, we have $\vec{S} = 0$.

In addition to these governing PDEs, this system requires boundary conditions, which are the focus of this brief. To motivate the discussion on boundary conditions, let's consider the case illustrated in Figure 1. A drop of phase 1, surrounded by phase 2, is touching the wall: A contact line is present. Let's now define the contact angle θ, the angle the interface makes with the wall boundary as measured through phase 1. What are the appropriate boundary conditions when a contact line is present? The condition $\partial \phi / \partial n_\mathrm{w} = 0$, where n_w is the coordinate in the wall-normal direction, directly enforces that $\theta = 90°$. This results in the desirable property of no diffusive or sharpening flux through the wall, but the equilibrium contact angle for an arbitrary combination of phases and a solid is not 90°. Rather, for a static drop, the equilibrium contact angle, θ_eq, is determined by Young's equation,

$$\gamma_{2s} - \gamma_{1s} - \gamma_{12}\cos(\theta_\mathrm{eq}) = 0, \tag{1.4}$$

where γ_{1s} is the surface tension coefficient of the interface between the solid and phase 1, γ_{2s} is of solid and phase 2, and γ_{12} is of phases 1 and 2. Enforcing the contact angle to be 90° is unphysical and undesirable. Therefore, the boundary condition $\partial \phi / \partial n_\mathrm{w} = 0$

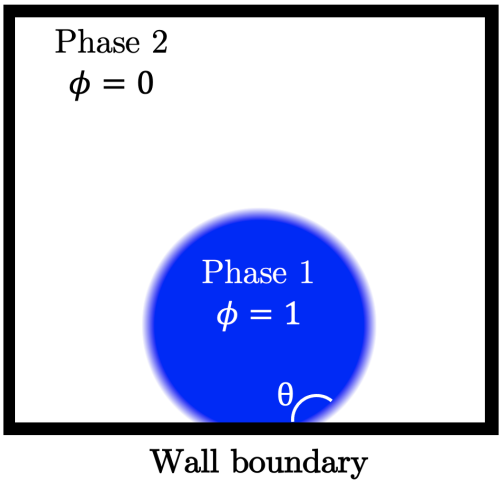

FIGURE 1. Schematic of a drop in the CDI model on a wall. Three-phase contact lines are present. The associated contact angle θ is the angle between the interface and the wall, measured through phase 1.

should be modified when contact lines are present. This condition enforces the diffusive and sharpening fluxes through the wall to be individually equal to zero. Alternatively, the no-flux condition can be achieved by setting their sum equal to zero. Namely, projecting the artificial flux onto n_{w} and setting it equal to zero gives

$$\left[\epsilon - \frac{\phi(1-\phi)}{|\nabla\phi|}\right]\frac{\partial\phi}{\partial n_{\mathrm{w}}} = 0, \tag{1.5}$$

which can be satisfied by either setting $\partial\phi/\partial n_{\mathrm{w}} = 0$ or by enforcing $\epsilon|\nabla\phi| = \phi(1-\phi)$. In this report, we choose the latter condition. Since the diffusive and sharpening fluxes are antiparallel, this condition requires that their magnitudes be equal at the wall. Furthermore, since this is a requirement on the magnitudes of the fluxes and not their direction, this condition can be satisfied with any contact angle θ.

The no-flux condition on ϕ is therefore amenable to a non-90° contact angle, but how can a particular contact angle be enforced? What changes are required so that θ attains the prescribed θ_{eq} at static equilibrium? Since CDI is second-order in space, there is only one boundary condition on the phase-field variable to apply at each wall. After enforcing the no-flux condition, there are no more degrees of freedom on the phase-field equation to restrict the contact angle. However, there is another degree of freedom in the boundary conditions on the Navier-Stokes equation. Rather than setting the typical no-slip condition, in this report, we use a slip boundary condition. This boundary condition is derived for CDI based on the Generalized Navier Boundary Condition (Qian *et al.* 2003), and we use numerical tests to demonstrate that it results in physical and desired behavior for static and moving contact lines. Note that this approach preserves local conservation of mass (i.e., ϕ), in contrast to treatments for second-order phase-field equations based on Lagrange multipliers, which only achieve global conservation of mass (Huang *et al.* 2022).

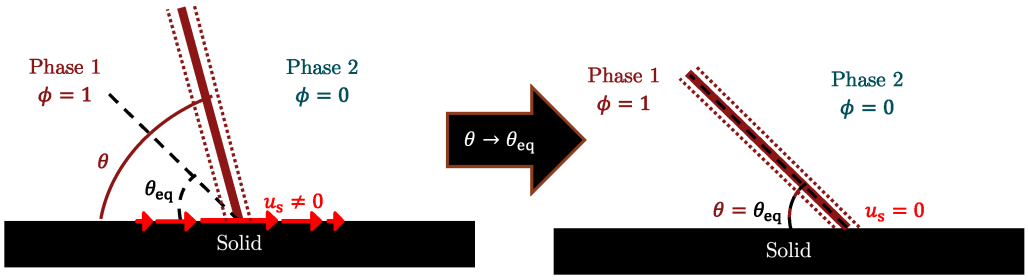

FIGURE 2. Schematic of the desired slip boundary condition. A slip velocity localized around the contact line advects the contact line to change the contact angle θ toward the equilibrium contact angle θ_{eq}.

2. Formulation of the slip boundary condition

The idea of a slip boundary condition to enforce static contact angles is illustrated in Figure 2. When $\theta \neq \theta_{eq}$, there should be advection of ϕ on the wall due to a slip velocity, such that $\theta \rightarrow \theta_{eq}$. When $\theta = \theta_{eq}$, this slip velocity should be zero. In addition, the slip velocity should be localized around the contact line so that this slip mechanism does not affect the flow where it is not needed.

Given this desired qualitative behavior of the slip velocity u_s, the question moves to its precise form. For this, we rely on the observations of extensive molecular dynamics simulations made by Qian *et al.* (2003). They found that the slip velocity near a moving contact line is given by

$$u_s = l_s \frac{\partial u_\tau}{\partial n_w} - \beta \sigma^{ST}. \tag{2.1}$$

The first term on the RHS is the classic Navier boundary condition, where l_s is the slip length and u_τ is the wall-tangential velocity component. For this report, we have chosen to set $l_s = 0$ in order to reduce the number of free parameters and isolate the effect of the second term, which we expect to be capable of modeling contact lines on its own. That second term consists of a tunable parameter β and a net surface tension stress (uncompensated Young's stress) σ^{ST} due to the deviation of the contact angle from its equilibrium value, which is given by

$$\sigma^{ST} = \gamma_{12}[\cos(\theta_{eq}) - \cos(\theta)] f(\phi). \tag{2.2}$$

The function $f(\phi)$ should be a smoothed Dirac delta function that peaks at the contact line and integrates to 1 across the interface. In addition, it should give u_s the correct sign depending on whether the contact line is advancing or receding. The following function for $f(\phi)$ satisfies these properties,

$$f(\phi) = 6\phi(1-\phi)\frac{\partial \phi}{\partial \tau}, \tag{2.3}$$

where τ denotes the wall-tangential coordinate. Substituting this into Eq. (2.1) and using the equilibrium profile for ϕ gives

$$u_s = l_s \frac{\partial u_\tau}{\partial n_w} - \beta \gamma_{12} \left[\epsilon \frac{\partial \phi}{\partial n_w} + \phi(1-\phi)\cos(\theta_{eq}) \right] \frac{\partial \phi}{\partial \tau}. \tag{2.4}$$

For completeness, the Navier boundary condition term is included in Eq. (2.4).

The choice of $f(\phi)$ is inspired by the sharpening term in Eq. (1.1), specifically the $\phi(1-\phi)$ factor. In their CH-NS results, Qian *et al.* (2003) note that the choice of the

peaked function has little effect on the final result, so other choices of $f(\phi)$ may work, but they have not been studied in this work.

3. Results

The slip boundary condition presented in Eq. (2.4) has been implemented within an in-house CDI solver (Mirjalili & Mani 2021). The calculations were made on a uniform staggered finite difference mesh with second-order central difference approximations in space. A third-order Runge-Kutta time-stepping scheme is used (Le & Moin 1991). Boundary conditions are implemented using the ghost cell method. In the calculations, the RHS flux is represented by a separate field, and the no-flux condition Eq. (1.5) is implemented by explicitly setting the RHS flux to be zero on the wall. In this section, we present two two-dimensional test cases.

3.1. *Test case 1: drop evolving to static equilibrium*

With the first test case, we seek to verify that the static contact angle of a drop on a solid wall equals the specified equilibrium contact angle θ_{eq} (Huang *et al.* 2022). Three different values of θ_{eq} were tested: 45°, 90° and 135°. For each value, a drop was initialized with a 90° contact angle in a zero velocity field and was allowed to evolve to a steady state. The horizontal and vertical directions are x and y, respectively, and the velocity components in those directions are u and v. The domain is given by $L_x = 1$ and $L_y = 0.5$, and the number of mesh points in each direction are $N_x = 200$ and $N_y = 100$. This gives the mesh size $h_x = h_y = h = 0.005$. The bottom boundary is a wall, with the no-flux boundary condition given by Eq. (1.5) and the slip boundary condition given by Eq. (2.4) applied. The slip boundary condition is applied for u, while the no-penetration condition is enforced on v. At the top boundary, no slip is applied. In addition, the Neumann boundary condition is applied to pressure at the top and bottom boundaries. All fields are periodic in the x direction. Finally, the parameter Γ appearing in Eq. (1.1) is set to be equal to 2.5 times the maximum velocity at a given time step (Mirjalili *et al.* 2020), and the following other parameters were used: $\epsilon = 0.0056$, $\gamma = 1$, $\rho_1 = \rho_2 = 0.01$, $\mu_1 = \mu_2 = 0.01$ and $\beta = 10$. The results are shown in Figure 3. The dashed red lines denote the exact solutions, set uniquely by conservation of mass and the desired contact angle of θ_{eq}. As the snapshots show, the drops evolve to the exact solution, thus providing evidence that the slip boundary condition given in Eq. (2.4) results in correct behavior for a static contact line.

Furthermore, a mesh refinement study has been conducted. Three measures of error at steady state are shown: i) the relative error in the length of the drop, ii) the relative error in the height of the drop and iii) the relative shape error. The relative shape error is defined as $\int |H_{\text{num}}(x,y) - H_{\text{exact}}(x,y)| / \int H_{\text{exact}}(x,y)$. $H(x,y)$ is the Heaviside function that is 1 within the drop and 0 outside. For the numerical solution, $H_{\text{num}} = 1$ if $\phi > 0.5$. Figure 4 shows that there is mesh convergence in all three quantities and that the convergence is around first order.

3.2. *Test case 2: Couette flow*

While the first test case shows that static contact lines are correctly modeled with the proposed slip boundary condition, the Couette flow test case provides a means of testing the behavior of moving contact lines. In this geometry, a square drop initialized in a zero velocity field is sheared by the top and bottom walls, which move in opposite directions and at the same speed. Again, tests were conducted at $\theta_{\text{eq}} = 45°$, 90° and 135°. Here,

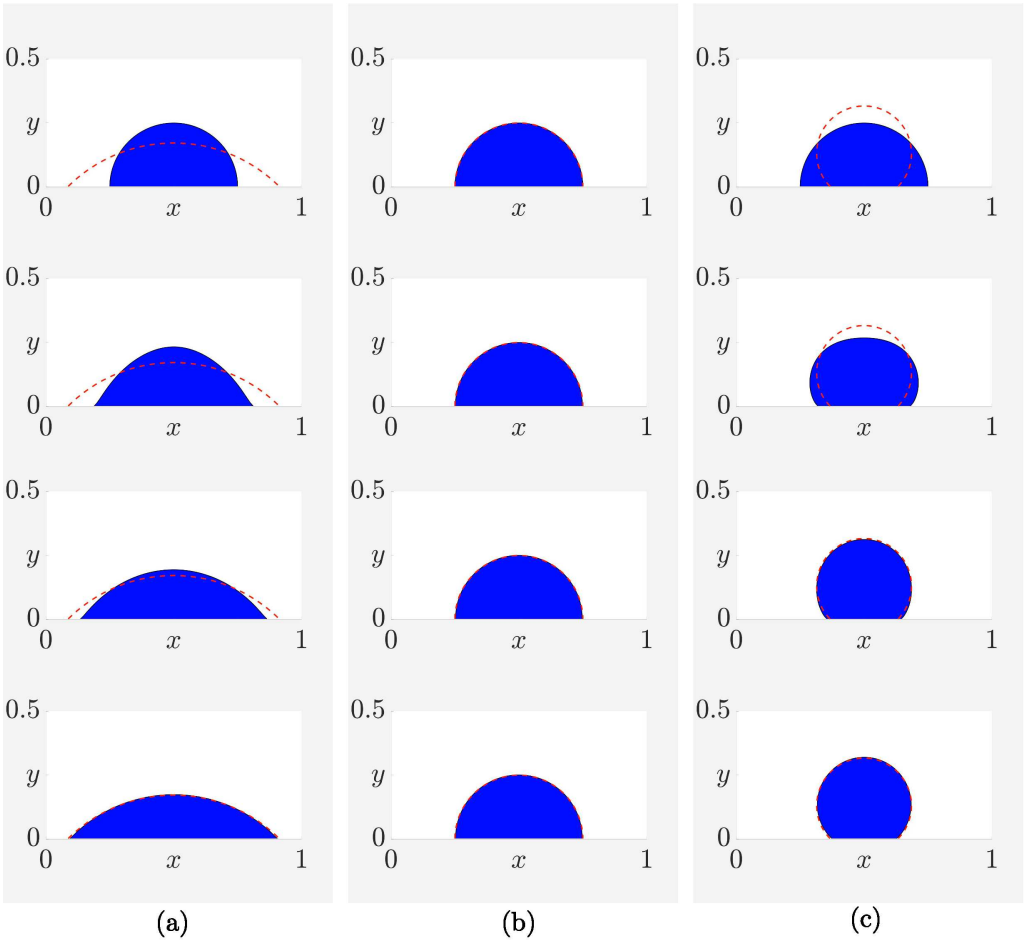

FIGURE 3. Snapshots of the evolution of a drop with a 90° initial contact angle and (a) a 45° equilibrium contact angle, (b) a 90° equilibrium contact angle and (c) a 135° equilibrium contact angle, shown against the exact steady-state solution represented with dashed red lines.

we have the capillary number $Ca = \mu U_w/\gamma = 1 \times 10^{-2}$, where U_w is the wall speed. All other simulation details are the same as in the first test case, except that the top and bottom boundaries are now walls and $\beta = 1$ in this test case. Snapshots of the results are shown in Figure 5. These snapshots illustrate the qualitative behavior of this slip boundary condition for moving contact lines. The initially square drop evolves to attain a contact angle that's close to θ_{eq}, but slightly different due to the shearing action of the walls, which tends to rotate the interfaces clockwise to be more horizontal. At steady state, the advancing contact lines (top left and bottom right of each drop) have $\theta > \theta_{eq}$ and the receding contact lines (top right and bottom left of each drop) have $\theta < \theta_{eq}$. This evolution agrees with previous results in the literature (Yue & Feng 2011; Qian *et al.* 2003).

In addition to simulations with various θ_{eq} at fixed Ca, we have also conducted simulations with various Ca at fixed $\theta_{eq} = 45°$. Ca is varied by varying U_w, while μ and γ are held constant. The steady-state results are shown in Figure 6. It is clear that as Ca

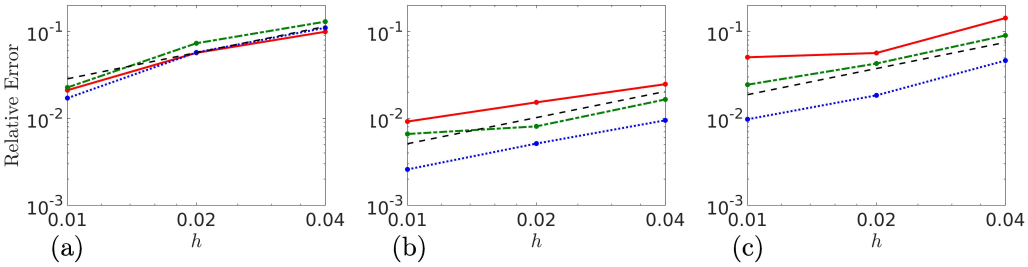

FIGURE 4. Relative error between the numerical and exact solutions as a function of the mesh size h, for the three different values of θ_{eq} tested: (a) 45°, (b) 90° and (c) 135°. The solid red, dotted blue and dash-dotted green lines are the length, height and shape error, respectively. The dashed line marks a slope of 1 corresponding to first-order convergence.

increases, the steady-state deformed configuration is more sheared. This trend is qualitatively in agreement with our expectations and previous results in literature (Yue & Feng 2011; Qian *et al.* 2003).

At this point, these Couette flow results are only qualitatively correct in that they capture the correct trends in interface position as θ_{eq} and Ca are varied. However, there is quantitative disagreement with previous results in literature (Qian *et al.* 2003). In particular, there is error in predicting the contact angle. In this work, the parameter β was chosen somewhat arbitrarily, and clearly, β must be tuned to provide quantitative agreement. This is reserved for future work. In addition, there are several possible improvements to the numerical implementation that will be explored in future work.

4. Conclusion

Defining the proper boundary conditions to capture contact-line physics is challenging when using a second-order phase-field method. In order to conserve mass, the no-flux condition on walls is applied to the phase field variable, but this prevents direct imposition of a contact angle. The contact angle can be restricted, however, by imposing a slip boundary condition on the Navier-Stokes equation. Such a boundary condition advects the phase-field variable on the wall in order to evolve the contact angle toward a prescribed equilibrium contact angle. By examining the static equilibrium of drops for various equilibrium contact angles, it has been shown that this slip boundary condition results in the correct static contact angle. Furthermore, the Couette flow test case demonstrates qualitatively correct behavior, while allowing us to calibrate the model in future work. Future work will be dedicated to formal derivation of the presented slip boundary condition, in addition to calibration of the free parameters and rigorous testing on canonical and realistic problems.

Acknowledgements

This investigation is supported by the NSF Graduate Research Fellowship Program and the Department of Energy, National Nuclear Security Administration under Award Number DE-NA0003968.

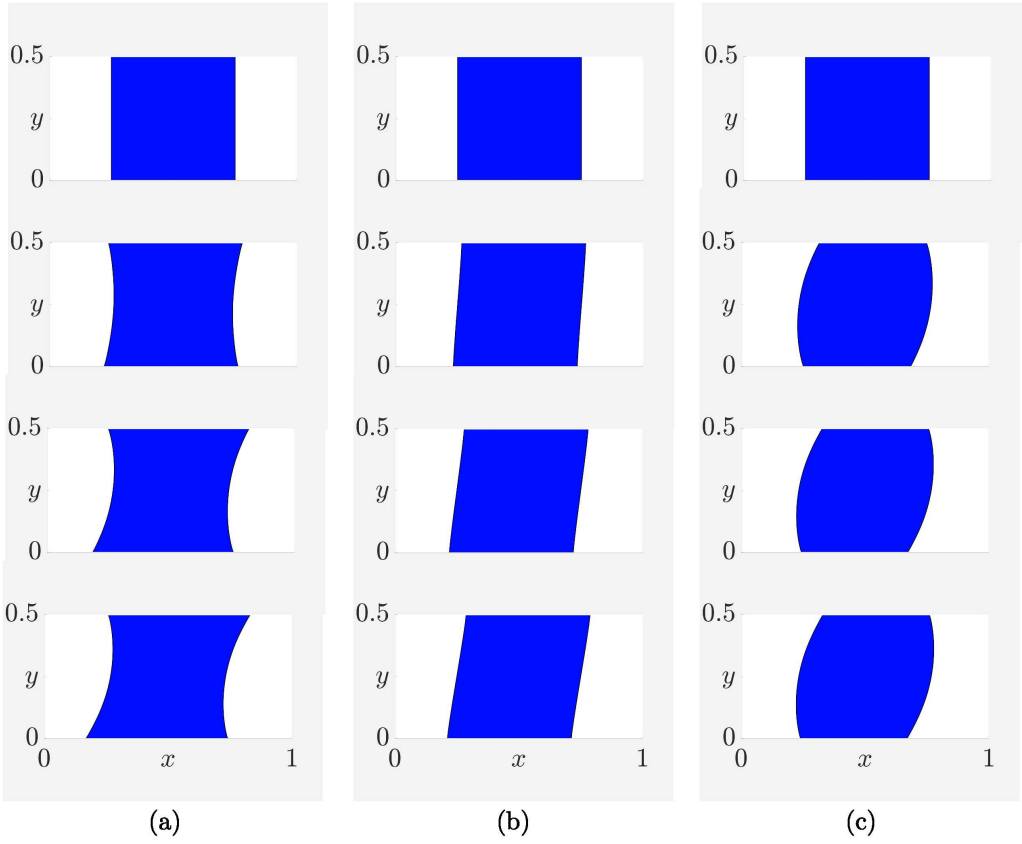

FIGURE 5. Snapshots of the evolution of an initially square drop subject to shear from the top and bottom walls, moving to the right and left, respectively, at $U_{wall} = 1$. This corresponds to a capillary number of $Ca = 1 \times 10^{-2}$. Three different values of θ_{eq} are shown: (a) 45°, (b) 90° and (c) 135°.

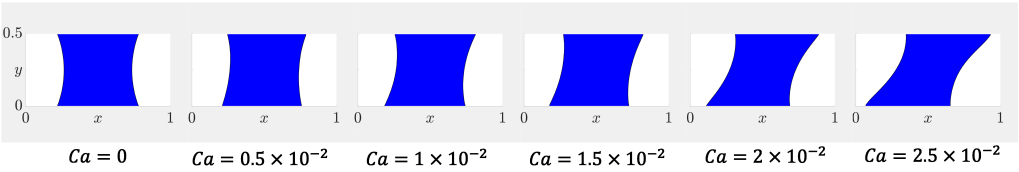

FIGURE 6. Couette flow at steady state, for $\theta_{\text{eq}} = 45°$ and various Ca.

REFERENCES

ABELS, H., GARCKE, H. & GRÜN, G. 2012 Thermodynamically consistent, frame indifferent diffuse interface models for incompressible two-phase flows with different densities. *Math. Mod. Meth. Appl. S.* **22** (03), 1150013.

CHIU, P. H. & LIN, Y. T. 2011 A conservative phase field method for solving incompressible two-phase flows. *J. Comput. Phys.* **230**, 185–204.

HUANG, Z., LIN, G. & ARDEKANI, A. M. 2022 Implementing contact angle boundary

conditions for second-order phase-field models of wall-bounded multiphase flows. *J. Comput. Phys.* **471**, 111619.

Jacqmin, D. 1999 Calculation of two-phase Navier–Stokes flows using phase-field modeling. *J. Comput. Phys.* **155** (1), 96–127.

Jain, S. S., Mani, A. & Moin, P. 2020 A conservative diffuse-interface method for compressible two-phase flows. *J. Comput. Phys.* **418**, 109606.

Khanwale, M. A., Lofquist, A. D., Sundar, H., Rossmanith, J. A. & Ganapathysubramanian, B. 2020 Simulating two-phase flows with thermodynamically consistent energy stable Cahn-Hilliard Navier-Stokes equations on parallel adaptive octree based meshes. *J. Comput. Phys.* **419**, 109674.

Le, H. & Moin, P. 1991 An improvement of fractional step methods for the incompressible Navier-Stokes equations. *J. Comput. Phys.* **92**, 369–379.

Magaletti, F., Picano, F., Chinappi, M., Marino, L. & Casciola, C. M. 2013 The sharp-interface limit of the Cahn–Hilliard/Navier–Stokes model for binary fluids. *J. Fluid Mech.* **714**, 95–126.

Mirjalili, S., Ivey, C. B. & Mani, A. 2019 Comparison between the diffuse interface and volume of fluid methods for simulating two-phase flows. *Int. J. Multiphas. Flow* **116**, 221–238.

Mirjalili, S., Ivey, C. B. & Mani, A. 2020 A conservative diffuse interface method for two-phase flows with provable boundedness properties. *J. Comput. Phys.* **401**, 109006.

Mirjalili, S., Jain, S. S. & Dodd, M. 2017 Interface-capturing methods for two-phase flows: An overview and recent developments. *Annual Research Briefs*, Center for Turbulence Research, Stanford University, pp. 117–135.

Mirjalili, S. & Mani, A. 2021 Consistent, energy-conserving momentum transport for simulations of two-phase flows using the phase field equations. *J. Comput. Phys.* **426**, 109918.

Mohammad Karim, A. 2022 A review of physics of moving contact line dynamics models and its applications in interfacial science. *J. Appl. Phys.* **132** (8), 080701.

Qian, T., Wang, X.-P. & Sheng, P. 2003 Molecular scale contact line hydrodynamics of immiscible flows. *Phys. Rev. E* **68**, 016306.

Shahmardi, A., Rosti, M. E., Tammisola, O. & Brandt, L. 2021 A fully Eulerian hybrid immersed boundary-phase field model for contact line dynamics on complex geometries. *J. Comput. Phys.* **443**, 110468.

Snoeijer, J. H. & Andreotti, B. 2013 Moving contact lines: scales, regimes, and dynamical transitions. *Annu. Rev. Fluid Mech.* **45** (1), 269–292.

Sui, Y., Ding, H. & Spelt, P. D. 2014 Numerical simulations of flows with moving contact lines. *Annu. Rev. Fluid Mech.* **46**, 97–119.

Yue, P. & Feng, J. J. 2011 Can diffuse-interface models quantitatively describe moving contact lines? *Eur. Phys. J. Spec. Top.* **197**, 37–46.